Macromolecules

Article

pubs.acs.org/Macromolecules

Improving the Gas Barrier Properties of Nafion via Thermal Annealing: Evidence for Diffusion through Hydrophilic Channels and Matrix

Christopher M. Evans,[†] Meenesh R. Singh,[‡] Nathaniel A. Lynd,[‡] and Rachel A. Segalman*[,†]

[†]Department of Chemical Engineering, University of California, Santa Barbara, Santa Barbara, California 93106, United States

[‡]Materials Science Division, Lawrence Berkeley National Laboratory, Berkeley, California 94720, United States

Supporting Information

ABSTRACT: Oxygen diffusion through commercial Nafion films is investigated using a transient electrochemical reduction method. Direct experimental evidence is found for two Fickian diffusion coefficients corresponding to oxygen permeation through the hydrophilic channels and fluorocarbon matrix. The diffusion coefficient and solubility of oxygen in each phase, which controls the overall permeability, can be tuned via thermal annealing where films annealed at 160 °C have a substantially reduced oxygen permeability relative to the as-received material. Films annealed at 200 °C show intermediate oxygen permeation to the as-received and 160 °C annealed samples. Differential scanning calorimetry and wide-angle X-ray scattering are employed to demonstrate that increasing crystallinity reduces the oxygen solubility and diffusion coefficient through the Nafion matrix. The two oxygen diffusion coefficients are discussed in the context of literature values which span more than an order of magnitude. It is found that the time scale of the experiments plays a substantial role in the measured diffusion coefficient with short time scale (<30 s) experiments sensing primarily diffusion through the hydrophilic channels. Longer time scale experiments (>300 s) are able to sense both modes of oxygen permeation.

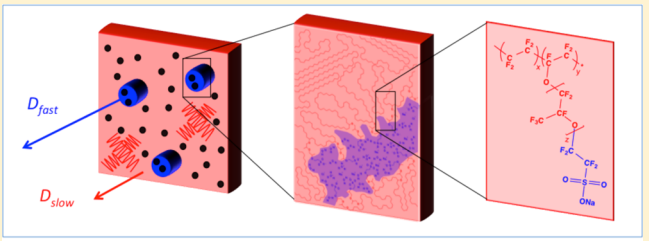

Nafion exhibits a heterogeneous morphology and commensurate dual-mode transport

INTRODUCTION

Nafion is a commercially available perfluorosulfonate ionomer used in polymer−electrolyte fuel cells,[1] chloralkali cells,[2] and solar fuels devices.[3] In the last application, water is oxidized to oxygen gas and protons at one electrode while protons are reduced to hydrogen gas on the opposite electrode.[4] The Nafion membrane serves as a path for ion conduction while simultaneously separating oxygen and hydrogen.[3] If the membrane is a poor gas barrier, oxygen will diffuse into the hydrogen stream creating a less pure product as well as a gas mixture which is in the explosive regime.[5] Hydrogen diffusion into the oxygen stream results in a loss of the desired product and can be oxidized in place of water, resulting in a lower current efficiency for hydrogen.[6] Requirements for low gas permeability are more strict in solar fuels devices than in fuel cells due to the much lower operating current densities.[6] Thus, it is of crucial importance to understand and control the permeation of gases through such membranes, yet a fundamental understanding of gas transport is lacking.

Gas diffusion in rubbery homopolymers is typically well described by a single Fickian diffusion coefficient[7] while diffusion in glassy polymers can exhibit "dual-mode" sorption.[8,9] In glassy polymers, these modes correspond to sorption of gas into the amorphous polymer matrix and into the free volume of the polymer, the latter process depending on the pressure of the diffusing gas. In Nafion membranes, diffusion of gases through the hydrophilic channels is thought to dominate the membrane permeability and is frequently described by a single Fickian diffusion coefficient.[10−18] Experimentally, literature values for oxygen diffusion coefficients (D) vary by more than an order of magnitude even for membranes with nominally the same water content.[10−18] It is important to understand why such a discrepancy exists in order to obtain a better fundamental understanding of diffusion through microphase separated membranes such as those used for solar fuels devices. Weber and Newman have indicated that the upper and lower bounds for steady state oxygen permeation should be that of pure water and of pure Teflon, respectively, depending on the water content of the membrane.[19] Oxygen permeation measurements for Nafion immersed in liquid cannot be simply performed using standard pressure rise measurements and thus require the use of a specialized sensing technique, the most common being electrochemical reduction of oxygen.[10−18,20−23] Fluorescence quenching of a dye in the presence of oxygen[24,25] and electron paramagnetic resonance[26,27] have also been used to measure oxygen diffusion coefficients in liquid saturated environments.

Received: March 18, 2015
Revised: April 29, 2015
Published: May 8, 2015

DOI: 10.1021/acs.macromol.5b00579
Macromolecules 2015, 48, 3303−3309

A key factor related to the range of D appears to be the time scale of the experiment. Electrochemical experiments using a potential step technique (PST), where the oxygen reduction current is monitored over <30 s following a step in electrode potential, report $D \sim (1-2) \times 10^{-6}$ cm^2/s.[13,15,17] Longer time scale chronoamperometry (CA) experiments, where the potential is held at mass transfer limited O_2 reduction conditions for >300 s, report $D \sim (2-7) \times 10^{-7}$ cm^2/s.[11,13,14] Additionally, the early studies of Ogumi et al.[11] using the CA method revealed a two-step process for hydrogen diffusion in Nafion although only the faster mode was analyzed. They suggested that the second mode might be related to diffusion through the fluorocarbon matrix. In phase-separated materials such as Nafion, two permeation modes may be anticipated due to gas sorption into each phase.[28] We hypothesize that experiments that occur over longer time scales (>300 s) can sense diffusion through both the hydrophilic and fluorocarbon domains of Nafion while short time scale experiments (<30 s) predominantly sense the faster diffusion through water channels.

Here, we measure the diffusion coefficient of oxygen in Nafion using the CA technique. Evidence for two diffusive modes is presented where distinct Fickian diffusion coefficients are observed for oxygen in the hydrophilic domains and in the fluorocarbon matrix of Nafion. We draw a distinction with the well studied "dual-mode" sorption in glassy polymers which occurs due to molecular-scale inhomogeneities and is described with a Langmuir-type sorption term. Rather, these two modes arise from the nanoscopically heterogeneous morphology of Nafion, and each exhibits an apparent Fickian behavior with Henry's law type sorption. The permeability of oxygen is shown to be tunable via thermal annealing with decreasing permeability relative to as-received Nafion. Annealing also leads to lower water uptake in the hydrophilic channels which further reduces the oxygen permeation of the membrane. We investigate the dependence of both modes on thermal annealing and morphology.

EXPERIMENTAL SECTION

Nafion membranes (Ion Power, Nafion1110), polystyrene (Aldrich, average M_w = 192 000 g/mol), and Teflon (McMaster Carr) were purchased commercially. Nafion was used either as-received or annealed in a vacuum oven for 24 h at the specified temperature. All membranes were then soaked in 0.1 M H_2SO_4 for 48 h prior to the diffusion measurement. Polystyrene membranes were made via hot pressing (140 °C, 2000 psi) while Teflon was purchased in sheet form.

Chronoamperometry (CA) experiments were performed as previously described where a platinum working electrode on the downstream face of a membrane registers a reduction current after oxygen is introduced into the upstream side and diffuses through the membrane.[10−12,15] The diffusion cell was purchased from PermeGear and consisted of two 8 mL half cells with a glass port on top of each half shown schematically in Figure 1.

A membrane was sandwiched between the two cells via an O-ring (2 cm diameter) and metal clamp. On the downstream face of the membrane, a 2 cm diameter platinum foil working electrode (Aldrich) was placed in direct contact with the membrane. A platinum mesh counter electrode (Alfa Aesar) was placed on the back wall of the downstream cell and a mini reference electrode (Ag/AgCl, 3.5 mm o.d., Pine Research) was placed in between the working and counter electrodes. The downstream side was then sealed with parafilm and vacuum grease. To begin each measurement, deoxygenated 0.1 M sulfuric acid (bubbled with nitrogen for 1 h) was added to the cell with a membrane clamped in the middle. Cyclic voltammetry sweeps were performed by varying the potential from 1.5 to −0.5 V until the oxidation and reduction waves no longer changed for subsequent sweeps, typically 5−10 sweeps as previously described.[13] This procedure ensures a similar electrode surface for each diffusion experiment. The working electrode was then held at 0.1 V versus the reference electrode to remove residual oxygen in the system and to remove dissolved oxygen from the membrane. After at least 5 h of equilibration in deoxygenated conditions, a solution of oxygen-saturated sulfuric acid (bubbled with oxygen for 1 h) was injected into the upstream side of the cell. This point was taken as the zero time point, and the current was subtracted off as baseline (typically 1−3 μA) following literature procedures.[14,10] The reduction current of oxygen was monitored as a function of time using a Bio-Logic VSP-300 potentiostat.

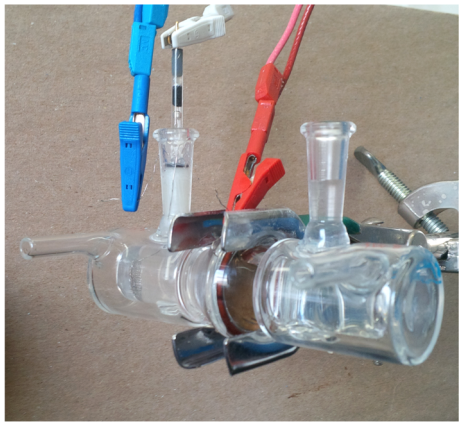

Figure 1. Photograph of the experimental setup. Red is attached to a working Pt foil electrode, blue is connected to a Pt mesh counter electrode against the back wall, and white is an Ag/AgCl reference electrode.

The solution to Fick's law has been previously solved for this geometry[20] and the transient oxygen reduction current ($i(t)$) can be fit to yield the oxygen diffusion coefficient (D) and oxygen solubility (S) of the membrane:

$$i(t) = \frac{n_e FADS}{s_{O_2} L}\left(\frac{2}{\sqrt{\pi\tau}}\right)\sum_{j=0}^{\infty}\exp\left[-\frac{(2j+1)^2}{4\tau}\right] \quad (1)$$

$$\tau = \frac{tD}{L^2} \quad (2)$$

where n_e is the number of electrons involved in oxygen reduction (2), F is Faraday's constant, A is the membrane area, s_{O_2} is the stoichiometry coefficient of oxygen (1/2), and L is the membrane thickness. Data were fit to eqs 1 and 2 using IgorPro software. Oxygen diffusion measurements using the electrochemical monitoring technique are shown in Figure 2 for a polystyrene (PS) homopolymer film. The oxygen reduction current was fit to a single Fickian diffusion process (red curve) and yielded an oxygen diffusion coefficient of 7×10^{-8} cm^2/s, in agreement with a literature value of 10×10^{-8} cm^2/s measured via a pressure rise method on a dry PS film.[29] Diffusion coefficients of $(2.3-4.3) \times 10^{-7}$ cm^2/s[30] and $(3.3-5.4) \times 10^{-7}$ cm^2/s[31] were obtained previously via luminescence methods. These PS data serve as a control experiment to verify that the measurement apparatus can provide reliable diffusion measurements. Figure 2b shows diffusion data for a sheet of commercial Teflon. In contrast to the PS film, Teflon cannot be well described by a single Fickian diffusion process (red curve). Previous investigations of small molecule dye diffusion in semicrystalline polypropylene have indicated that the sum of two Fickian diffusion coefficients is required to describe the dye diffusion through both the amorphous and crystalline regions of the polymer.[32] A sum of two Fickian diffusion modes to the present Teflon data provides a substantially improved fit with slow and fast diffusion coefficients of $D_{slow} = 3.3 \times 10^{-8}$ and $D_{fast} = 1.1 \times 10^{-7}$ cm^2/s, respectively. Previous work[24] measuring oxygen diffusion in Teflon

DOI: 10.1021/acs.macromol.5b00579
Macromolecules 2015, 48, 3303−3309

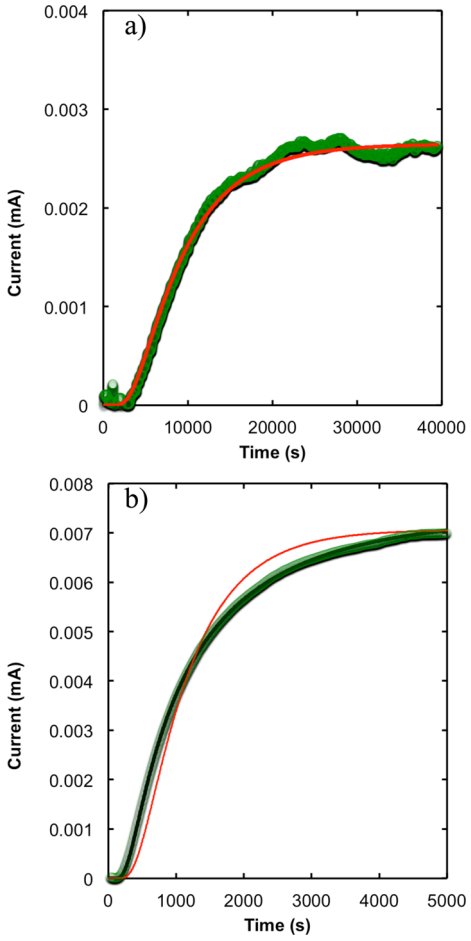

Figure 2. Electrochemical monitoring of oxygen diffusion through homopolymers. (a) Oxygen diffusion in a PS film (650 μm) can be fit to a single Fickian diffusion process (solid red curve) as expected for this amorphous material. (b) Oxygen diffusion in Teflon (230 μm) does not fit acceptable to a single Fickian mode (solid red curve) while the sum of two Fickian processes captures the full data set (solid black curve). The two processes correspond to diffusion in amorphous and near-crystalline regions.[30]

reported $D = 1.7 \times 10^{-7}$ cm^2/s via the time lag method where deviation from the baseline may be expected to correspond more closely to the fast diffusion process. A value of $D = 1.5 \times 10^{-7}$ cm^2/s was determined for oxygen in Teflon via pressure rise methods.[33] In fact, the time lag value agrees with D_{fast} observed in the present work. Thus, the chronoamperometry (CA) technique is a reliable method for determining oxygen diffusion coefficients in agreement with conventional pressure-based diffusion measurements.

Differential scanning calorimetry (TA Instruments, Q20) was performed on ~5 mg samples of Nafion at a heating rate of 20 °C/min. Annealed Nafion was removed from the vacuum oven at the annealing temperature and allowed to cool for 30 min before loading into a hermetically sealed aluminum pan. Acid-swollen Nafion films were patted dry with a KimWipe and promptly loaded into a hermetically sealed pan for DSC analysis. The instrument was calibrated with an ~6 mg indium standard.

Wide-angle X-ray scattering was performed at the Advanced Light Source, Lawrence Berkeley National Lab at beamline 7.3.3. The line is equipped with a 2D Dectris Pilatus 1 M charge-coupled device detector (981 × 1043 pixels). The incident X-rays had a wavelength of 1.24 Å. Acid-swollen Nafion samples were sandwiched between two pieces of Kapton tape immediately after removal from sulfuric acid. Scattering patterns were taken within 20 min of sample preparation.

Water uptake measurements were performed on Nafion of various thermal treatments to determine the volume fraction of hydrophilic domains. As-received Nafion as well as films annealed at 160 or 200 °C for 24 h were immersed in 0.1 M H_2SO_4 for 48 h. The membranes were patted dry with a KimWipe and promptly weighed. The films were then placed in a vacuum oven at 200 °C for 24 h to remove water and the dry mass was measured. The films were also measured after 48 h at 200 °C to ensure that 24 h was sufficient for water removal. The fractional mass uptake was determined as $w = (m_{wet} - m_{dry})/m_{dry}$, and the hydrophilic domain volume fraction (ϕ_v) was determined from the mass uptake, density of the dry membrane (ρ_{dry} = 2.0 g/cm^3),[34] and the density of water (ρ_{H_2O} = 1.0 g/cm^3) as[35]

$$\phi_v = \frac{\rho_{dry}}{\rho_{H_2O}} w \tag{3}$$

The fractional mass uptake was 0.181, 0.151, and 0.143 for as-received, annealed at 160 °C, and annealed at 200 °C Nafion. These correspond to ϕ_v = 0.36, 0.30, and 0.29, respectively.

RESULTS AND DISCUSSION

Diffusion of gases in homogeneous polymers is typically described by a gas solubility (S) and diffusion coefficient (D) with the permeability defined as $P = SD$. In multiphase polymer, nonhomogeneous sorption and diffusion behavior has been reported where each phase contributes to the overall permeation. The total permeation through a heterogeneous membrane is the sum of permeations from each possible mode (P_i) as written by Petropoulos:[28]

$$P = \sum P_i = \sum S_i D_i \tag{4}$$

Each P_i is the product of the solubility (S_i) and diffusion coefficient (D_i) for that mode. It is posited that any phase-separated membrane should exhibit a diffusion coefficient corresponding to each phase provided they are different enough to be resolved by experiments. In polymer blends and block copolymers, these permeation modes are weighted by their respective volume fractions.[28] Depending on the morphology, these modes may also be treated as being in series or parallel. In Nafion, two Fickian processes are anticipated corresponding to permeation through the hydrophilic and fluorocarbon regions of the material. The permeation is treated as a parallel combination of modes which captures the shape of the data quantitatively. Figure 3a shows data for oxygen diffusion through a Nafion1110 film. A fit to a single Fickian diffusion process (red dashed curve) cannot capture both the fast initial rise in the data and the longer time plateau region. A plot of the short time data is shown in Figure 3b, highlighting the inability of a single Fickian diffusion coefficient to fit the data. A sum of two Fickian processes provides an improved fit to the data and can be physically rationalized in terms of the two distinct environments present in Nafion. To incorporate both modes, the current is analyzed as $i(t) = i_{fast} + i_{slow}$ in accordance with eq 3, and each component takes the form of eq 1 with a distinct D and S. Such a treatment assumes both modes of diffusion are independent, which appears to be a valid assumption given the fit of the data using noninteracting modes. The case of interacting modes may become important in other systems such as glassy polymers as discussed previously.[36] The fast diffusion coefficient was determined as $D_{fast} = 1.4 \times 10^{-6}$ cm^2/s, in agreement with literature values of $D = 1.1 \times 10^{-6}$,[15] 1.9×10^{-6},[13] and 2.6×10^{-6} cm^2/s,[17] which employed a potential step technique (PST) where the transient current is monitored for <30 s.[10] The slow diffusion coefficient measured in the

DOI: 10.1021/acs.macromol.5b00579
Macromolecules 2015, 48, 3303−3309

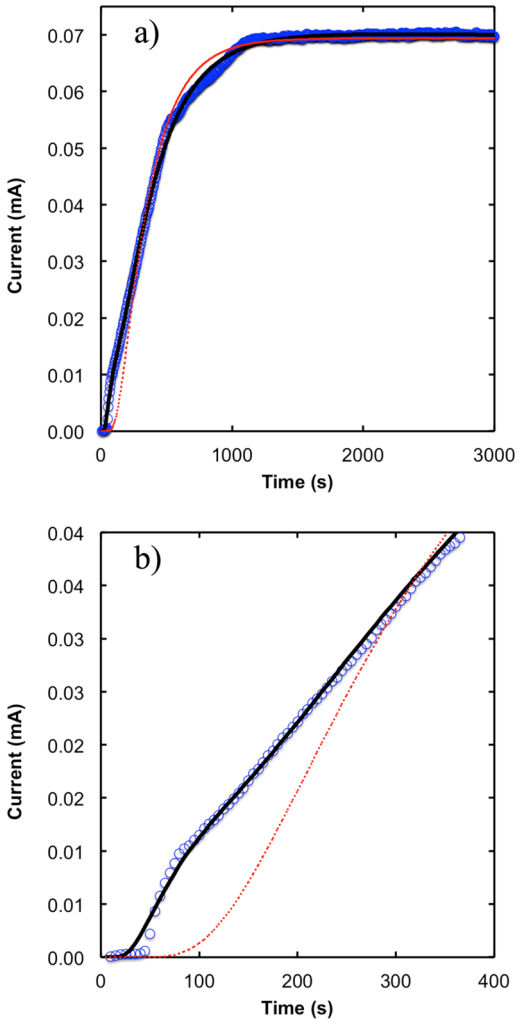

Figure 3. Oxygen diffusion through as-received Nafion 1110 (267 μm) monitored by electrochemical reduction method. (a) A single Fickian process (red dashed curve) does not capture the short time rise appropriately. The sum of two Fickian processes (black curve) provides a better fit and can be rationalized as representing diffusion through the hydrophilic and hydrophobic domains of Nafion. (b) Same data as (a) zoomed in to the short time region to illustrate discrepancies between the data and a single Fickian diffusion coefficient.

present work, D_{slow} = 3.0 × 10^{-7} cm^2/s, is in agreement with oxygen diffusion coefficients in Nafion of D = 2.4 × 10^{-7},[11] to 6.2 × 10^{-7},[14] to 7.0 × 10^{-7} cm^2/s[13] measured using the same CA technique as in the present work. We note that the diffusion coefficient of oxygen in bulk water has been reported as 29.5 × 10^{-6} cm^2/s,[11] substantially faster than any of the oxygen diffusion coefficients reported in Nafion. It is interesting that D_{fast} for Nafion is similar to the reported diffusion coefficient for water in Nafion channels (∼(1−7) × 10^{-6} cm^2/s) based on a number of studies discussed in detail in ref 37. It is not clear at the present time what the role of specific interactions between oxygen and the hydrophilic channels may be, and the relationship between oxygen and water diffusion warrants further study.

Each permeation mode P_i has a corresponding S_i which depends on the choice of electrode area A in eq 1. The area of the electrode used to calculate the solubility of oxygen for each mode was determined based on the volume fraction of each phase from water uptake measurements as described in the Experimental Section. For example, as-received Nafion has ϕ_v = 0.36, and thus the area used to calculate the solubility for the water hydrated channels, S_{fast}, is the geometric area of the Pt working electrode (3.14 cm^2) multiplied by 0.36. The solubility of 0.56 × 10^{-6} mol/cm^3 for S_{fast} is in agreement with the reported solubility of O_2 in dilute H_2SO_4 of 1 × 10^{-6} mol/cm^3.[38] The solubility of O_2 measured for the slow mode, S_{slow}, is 2.6 × 10^{-6} mol/cm^3, in agreement with previous CA literature values of 18.7× 10^{-6},[14] 13× 10^{-6},[13] and 7 × 10^{-6} mol/cm^3.[11]

Our findings indicate that the discrepancy in oxygen diffusion coefficients in Nafion is related to the time scale of the experiment. The potential step method, where the transient current response due to oxygen reduction is monitored over tens of seconds, may be sensitive primarily to the fast diffusion process while the longer time scale CA method senses contributions from both the slow and fast diffusion processes. In fact, Lehtinen et al.[13] used both of these electrochemical methods on Nafion 117 and found diffusion coefficients of 1.7 × 10^{-6} and 7 × 10^{-7} cm^2/s for the potential step and CA methods, respectively, supporting our assertion that the step method does not appropriately sense the slower diffusive mode. Previous work on gas diffusion in styrene−butadiene block copolymers found that short time scale transient experiments counted the diffusion of penetrants primarily from the PB matrix while a longer time scale "equilibrium method" also counted species diffusing through the PS domains.[39] For steady-state permeation measurements, series and parallel resistance models have been employed to account for diffusion through phase-separated block copolymers,[40,41] polymer blends,[42] and composite membranes[43] using permeabilities determined independently for each component. Our work differs from these studies in that we measure the transient response as opposed to steady state permeability.

Evidence for two diffusive modes in Nafion has appeared in the literature although it has scarcely been discussed. In the early work of Ogumi et al.[12] using the CA technique, it was observed that there were two steps in the data corresponding to diffusion of hydrogen in Nafion; however, only the faster of the two processes was analyzed. Sethuraman et al.[10] investigated CO and H_2S diffusion in Nafion, and inspection of their reduction current data also reveals two apparent steps which were fit to a single Fickian diffusion coefficient. Recent work on diffusion in anion exchange membranes using ^1H NMR has revealed multiple diffusion coefficients corresponding to the distinct environments within the membrane.[44] Interestingly, one might anticipate that Nafion would show three modes: one for the hydrophilic channels and two for the matrix corresponding to diffusion through amorphous regions and near-crystal regions (Figure 2b). A fit to three Fickian modes did not substantially improve the fit in Figure 3 likely due to the lower crystallinity of Nafion (8−12%)[45] relative to Teflon (∼70%).[46] The permeation mode arising from interactions with crystallites which is pronounced in Teflon (Figure 2b) would thus be significantly smaller in Nafion.

Thermal annealing is a facile route for tuning the morphology of polymer membranes and can be used to decrease gas permeability. In particular, increased percent crystallinity and crystal size can be achieved which is anticipated to substantially improve gas barrier properties. First, an increase in the crystallinity of the matrix should lead to a lower oxygen solubility as gases are much more soluble in amorphous domains.[47] Second, larger crystallites will act as barriers and

DOI: 10.1021/acs.macromol.5b00579
Macromolecules 2015, 48, 3303−3309

increase the tortuosity of the diffusion path for gas molecules. Additionally, annealing has been shown to limit water uptake into the hydrophilic channels of Nafion.[48] Thus, multiple morphological changes occur upon thermal treatment which impact oxygen permeability.

The morphological changes that accompany thermal annealing can be probed via differential scanning calorimetry (DSC). Figure 4 shows the DSC trace for Nafion with the

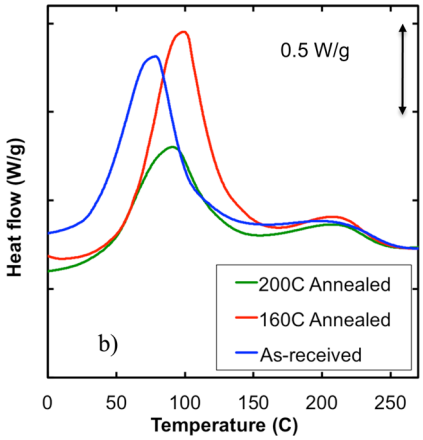

Figure 4. Role of thermal annealing on DSC characteristics of Nafion 1110. DSC traces (endotherm up) for Nafion as-received (top blue curve), annealed at 160 °C for 24 h (middle red curve), and annealed at 200 °C for 24 h (bottom green curve) after soaking in 0.1 M sulfuric acid for 48 h. The melting peak shifts to higher temperatures upon annealing at 160 °C due to an increase in crystal size. The width of the peak decreases upon annealing at 200 °C as smaller crystallites are melted.

various thermal treatments. Two bumps are observed with peaks at ∼75 and ∼200 °C for the as-received film (blue curve). Previous DSC work on Nafion (in Cs^+ form rather than H^+ form as in the present work) also observed two peaks but at slightly higher temperatures, at ∼100 and 250 °C.[48] In that work, the lower temperature peak shifted to higher temperature with annealing and eventually merged with the higher temperature peak. The peaks were assigned to smaller crystallites (lower temperature) which melt and then re-form onto larger crystallites which melt at higher temperature. Figure 4 also shows DSC for Nafion annealed at 160 °C (red curve) where the first peak is shifted to higher temperature and is greater in magnitude. In the context of previous work,[49] this could be interpreted as a growth of larger crystals at the expense of smaller ones. Annealing at 200 °C (green curve) leads to a reduction in the first peak intensity; however, it still occurs at a higher temperature than for the as-received material.

An assignment of the relative percent crystallinity is difficult via DSC not only because of the presence of two peaks but also due to the background which appears to be elevated above baseline. The heat of fusion for Teflon is commonly used to determine Nafion crystallinity. Because Nafion melts at a much lower temperature and has two broad endothermic peaks rather than a sharp transition, it is unclear how appropriate the use of Teflon heat of fusion is for determining Nafion crystallinity. It is also unclear if the two peaks in the DSC represent distinct crystal populations or a melt−recrystallization type phenomena as suggested by Page et al.[49] The absorbed water in Nafion also contributes to the baseline. Taking the area under the curves from 0 to 300 °C using a simple linear baseline, the areas are 373, 459, and 305 J/g for as-received, 160 °C annealed, and 200 °C annealed films, respectively. These give unphysically large results simply using the enthalpy of fusion for Teflon (which ranges from 54 to 104 J/g). The percent increase in the area under the curve for the 160 °C film relative to as-received is 23% while the permeation through the matrix (D_{slow}·S_{slow}) drops by ∼50%. It is not only the percent crystallinity which is important but also the crystal morphology. For example, the film annealed at 200 °C has a smaller area under the curve than the as-received sample, but the first peak is shifted to higher temperature. A simple interpretation would be that some of the crystals have melted, but the remaining crystallites are larger and have a higher peak melting temperature. Thus, we turn to WAXS for a complementary method for probing crystallinity.

Figure 5 shows WAXS data for Nafion films with the same annealing and soak treatments as those in Figure 4. A peak at q

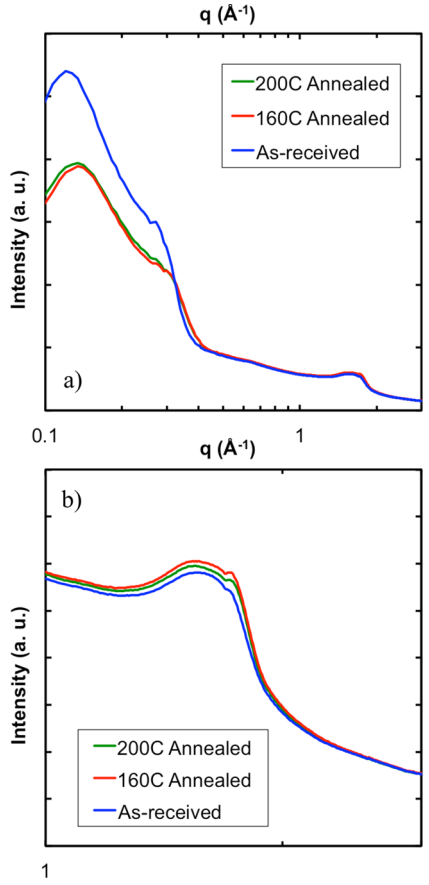

Figure 5. (a) WAXS traces for Nafion1110 as-received (blue curve), annealed at 160 °C (red curve), and annealed at 200 °C (green curve). Both the ionomer peak (q = 0.12 $Å^{-1}$) and the crystalline peak (q = 1.6 $Å^{-1}$) are visible in this range. The ionomer peak is weaker for the annealed samples due to reduced water uptake. (b) Enhancement of the higher q peak corresponding to matrix crystallinity for the same samples. The sample annealed at 160 °C has the highest crystallinity followed by the 200 °C annealed sample. As-received Nafion has the lowest crystallinity.

= 1.6 $Å^{-1}$ corresponds to crystallites in the matrix and has appears with a broad amorphous halo (Figure 5b) as previously reported for proton form Nafion.[34] As-received Nafion exhibits the lowest crystallinity followed by the sample annealed at 200 °C and finally that annealed at 160 °C. The highest crystallinity of the matrix phase in the 160 °C sample should result in the

DOI: 10.1021/acs.macromol.5b00579
Macromolecules 2015, 48, 3303−3309

lowest S_{slow} in this film. The WAXS data have been fit using two Gaussian peaks (Figure S3), and the percent crystallinity was taken as the ratio of the crystal peak area to the total area of crystalline plus amorphous regions. The crystallinity increases from 9.8% (as-received) to 10.6% (200 °C anneal) to 11.4% (160 °C anneal) in accord with our DSC interpretation and the order of diffusion coefficients through the matrix (although the effect is small). The q-range of the data in Figure 5a also includes the ionomer peak at q = 0.12 Å^{-1}, which is controlled by the uptake of water into the hydrophilic channels. The highest water uptake is observed for the as-received film while the lowest uptake is observed for the film annealed at 160 °C. The stronger ionomer peak in the as received Nafion is correlated with the greater D_{fast} in this membrane.

The changes in crystallinity due to annealing lead to substantial changes in the permeability of Nafion membranes. Figure 6 shows diffusion data for Nafion as a function of annealing time with the top blue curve corresponding to the as-received film presented in Figure 3. The bottom red curve is for Nafion that was annealed under vacuum at 160 °C for 24 h and then immersed in 0.1 M H_2SO_4 for 48 h prior to measurement. A fit to the data allows for the determination of D_{fast} = 4.7 and D_{slow} = 2.0 × 10^{-7} cm^2/s. The solubilities corresponding to the hydrophilic channels and matrix phase are S_{fast} = 1.1 and S_{slow} = 2.3 × 10^{-6} mol/cm^3, respectively. The lower solubility of gas in the matrix phase (S_{slow}) relative to as-received Nafion is attributed to increased crystallinity as seen via WAXS. Additionally, D_{slow} decreases presumably due to larger crystallite obstacles in the matrix. Water uptake into the ionic channels is also suppressed by the presence of a more crystalline matrix[48] which leads to a dryer and less mobile channel phase (lower D_{fast}). Interestingly, the oxygen solubility of the channels increases with decreasing water content. This is anticipated given that previous work[11] has reported that the solubility of oxygen is greater in Teflon than in water by a factor of 20. Lower water content leads to a more Teflon-like phase with increased oxygen solubility. Table 1 contains a summary of S and D values for the fast and slow modes in as-received and annealed Nafion films.

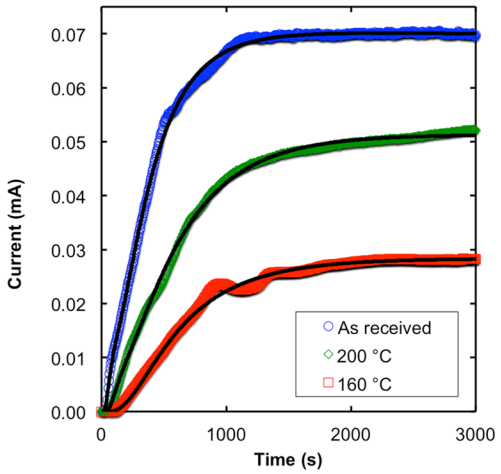

Figure 6. Role of thermal annealing on oxygen diffusion in Nafion as-received (top blue curve), annealed at 160 °C (bottom red curve), and annealed at 200 °C (middle green curve). All curves are fit to a sum of two Fickian modes. Substantially reduced oxygen permeability is observed upon annealing at 160 °C due to an increase in matrix crystallinity and a reduction in water uptake. The 200 °C annealed film reports intermediate permeation behavior due to an intermediate level of matrix crystallinity.

The choice of annealing temperature is important for gas permeation as exceedingly high temperatures can melt crystals that were present after lower temperature annealing conditions. The middle green curve in Figure 6 corresponds to a Nafion film annealed at 200 °C for 24 h followed by immersion in 0.1 M H_2SO_4 for 48 h. The permeation of oxygen shows intermediate behavior to the as-received and 160 °C annealed cases. This is attributed to an increase in the solubility of oxygen in the matrix phase due to the partial melting of crystals (as observed by DSC and WAXS) leading to a more amorphous matrix and thus higher S_{slow} relative to the 160 °C annealing case. We note that a discoloration was observed in the Nafion films as they turned orange/brown upon annealing. Ionic conductivity measurements were performed on all of the samples as a proxy for how many sulfonic acid sites had degraded. Conductivities of 74, 66, and 59 mS/cm were observed for the as-received, 160 °C annealed, and 200 °C annealed films. In addition to being only modestly different, they exhibit a monotonic decrease while permeation data are nonmonotonic. The conductivities are already anticipated to be slightly lower in annealed films due to the lower water uptake, indicating that degradation effects are minimal and not the reason for the decreased permeability seen in annealed membranes.

In conclusion, direct experimental evidence is presented for two Fickian modes of diffusion in Nafion. Two diffusion coefficients are observed corresponding to oxygen permeating through the hydrophilic channels and fluorocarbon matrix. The diffusion and solubility of oxygen in each phase, which controls the overall permeability, can be tuned via thermal annealing where films annealed at 160 °C have a substantially reduced oxygen permeability. Films annealed at 200 °C show intermediate oxygen permeation to the as-received and 160 °C annealed samples. Oxygen solubility in the matrix is determined by matrix crystallinity while the oxygen solubility in the hydrophilic channels is controlled by the water uptake. Future work is underway to investigate the performance of these annealed membranes in functional solar fuels devices.

■ ASSOCIATED CONTENT

Supporting Information

Figures S1−S3. The Supporting Information is available free of charge on the ACS Publications website at DOI: 10.1021/acs.macromol.5b00579.

Table 1. Solubility and Diffusion Coefficients for the Fast and Slow Diffusion Processes in Nafion

Nafion 1110	S_{fast} (× 10^6 mol/cm^3)	D_{fast} (× 10^6 cm^2/s)	S_{slow} (× 10^6 mol/cm^3)	D_{slow} (× 10^6 cm^2/s)
as received	0.56 ± 0.18	1.4 ± 0.37	2.6 ± 1.3	0.30 ± 0.04
annealed 160 °C	1.1 ± 0.80	0.47 ± 0.23	2.3 ± 1.9	0.20 ± 0.14
annealed 200 °C	0.15 ± 0.05	0.57 ± 0.08	4.1 ± 2.9	0.25 ± 0.08

DOI: 10.1021/acs.macromol.5b00579
Macromolecules 2015, 48, 3303−3309

AUTHOR INFORMATION

Corresponding Author

*E-mail: segalman@engineering.ucsb.edu (R.A.S.).

Notes

The authors declare no competing financial interest.

ACKNOWLEDGMENTS

This material is based on work performed by the Joint Center for Artificial Photosynthesis, a DOE Energy Innovation Hub, supported through the Office of Science of the U.S. Department of Energy under Award DE-SC0004993. We thank Dr. Daniel J. Miller, Dr. Adam Z. Weber, and Prof. Bryan D. McCloskey for helpful discussions.

REFERENCES

(1) Mauritz, K. A.; Moore, R. B. *Chem. Rev.* **2004**, *104*, 4535.
(2) Grot, W. *Chem.-Ing.-Tech.* **1978**, *50*, 299.
(3) Modestino, M. A.; Walczak, K. A.; Berger, A.; Evans, C. M.; Haussener, S.; Koval, C. A.; Newman, J. S.; Ager, J. W.; Segalman, R. A. *Energy Environ. Sci.* **2014**, *7*, 297−297.
(4) Nocera, D. G.; Lewis, N. S. *Proc. Natl. Acad. Sci. U. S. A.* **2006**, *103*, 15729.
(5) Schröder, V.; Emonts, B.; Janssen, H.; Schulze, H. P. *Chem. Eng. Technol.* **2004**, *27*, 847−851.
(6) Berger, A.; Segalman, R. A.; Newman, J. S. *Energy Environ. Sci.* **2014**, *7*, 1468.
(7) Masaro, L.; Zhu, X. X. *Prog. Polym. Sci.* **1999**, *24*, 731−775.
(8) Paul, D. R.; Koros, W. J. *J. Polym. Sci., Polym. Phys. Ed.* **1976**, *14*, 675−685.
(9) Barrer, R. M. *J. Membr. Sci.* **1984**, *18*, 25−35.
(10) Sethuraman, V. A.; Khan, S.; Jur, J. S.; Haug, A. T.; Weidner, J. W. *Electrochim. Acta* **2009**, *54*, 6850−6860.
(11) Ogumi, Z.; Takehara, Z.; Yoshizawa, S. *J. Electrochem. Soc.* **1984**, *I*, 769−773.
(12) Ogumi, Z.; Kuroe, T.; Takehara, Z. *J. Electrochem. Soc.* **1985**, *132*, 2601−2605.
(13) Lehtinen, T.; Sundholm, G.; Holmberg, S. *Electrochim. Acta* **1998**, *43*, 1881−1890.
(14) Haug, A. T.; White, R. E. *J. Electrochem. Soc.* **2000**, *147*, 980−983.
(15) Gode, P.; Lindbergh, G.; Sundholm, G. *J. Electroanal. Chem.* **2002**, *518*, 115−122.
(16) Beattie, P. D.; Basura, V. I.; Holdcroft, S. *J. Electroanal. Chem.* **1999**, *468*, 180−192.
(17) Buchi, F. N.; Wiakizoe, M.; Srinivasan, S. *J. Electrochem. Soc.* **1996**, *143*, 927.
(18) Basura, V. I.; Beattie, P. D.; Holdcroft, S. *J. Electroanal. Chem.* **1998**, *458*, 1.
(19) Weber, A. Z.; Newman, J. *J. Electrochem. Soc.* **2004**, *151*, A311−A325.
(20) Fan, D.; White, R. E.; Gruberger, N. *J. Appl. Electrochem.* **1992**, *22*, 770−772.
(21) Parthasarathy, A.; Martin, C. R.; Srinivasan, S. J. *Electrochem. Soc.* **1991**, *138*, 916−921.
(22) Parthasarathy, A.; Srinivasan, S.; Appleby, A. J.; Martin, C. R. *J. Electrochem. Soc.* **1992**, *139*, 2530.
(23) Yeo, R. S.; McBreen, J. *J. Electrochem. Soc.* **1979**, *126*, 1682−1687.
(24) Rharbi, Y.; Yekta, A.; Winnik, M. A. *Anal. Chem.* **1999**, *71*, 5045−5053.
(25) Yargi, O.; Ugur, S.; Pekcan, O. *J. Fluoresc.* **2013**, *23*, 357.
(26) Hatcher, M. E.; Plachy, W. Z. *Biochim. Biophys. Acta* **1993**, *1149*, 73−8.
(27) Smirnov, A. I.; Clarkson, R. B.; Belford, R. L. *J. Magn. Reson., Ser. B* **1996**, *111*, 149−157.
(28) Petropoulos, J. H. *Adv. Polym. Sci.* **1985**, *64*, 93.
(29) Weir, N. A. *J. Macromol. Sci., Part B: Phys.* **1975**, *B11*, 553.
(30) Gao, Y.; Baca, A. M.; Wang, B.; Ogilby, P. R. *Macromolecules* **1994**, *27*, 7041−7048.
(31) Bowyer, W. J.; Xu, W.; Demas, J. N. *Anal. Chem.* **2004**, *76*, 4374−4378.
(32) Quijada-Garrido, I.; Barrales-Rienda, J. M.; Frutos, G. *Macromolecules* **1996**, *29*, 7164−7176.
(33) Pasternak, R. A.; Christensen, M. V.; Heller, J. *Macromolecules* **1970**, *3*, 366.
(34) Gierke, T. D.; Munn, G. E.; Wilson, F. C. *J. Polym. Sci., Polym. Phys. Ed.* **1981**, *19*, 1687−1704.
(35) Kim, M.-H.; Glinka, C. J.; Grot, S. A.; Grot, W. G. *Macromolecules* **2006**, *39*, 4775.
(36) Fredrickson, G. H.; Helfand, E. *Macromolecules* **1985**, *18*, 2201−2207.
(37) Zhao, Q.; Majsztrik, P.; Benzinger, J. *J. Phys. Chem. B* **2011**, *115*, 2717−2727.
(38) Gubbins, K. E.; Walker, R. D. *J. Electrochem. Soc.* **1965**, *112*, 469.
(39) Odani, H.; Taira, K.; Nemoto, N.; Kurata, M. *Polym. Eng. Sci.* **1977**, *17*, 527−534.
(40) Kofinas, P.; Cohen, R. E.; Halasa, A. F. *Polymer* **1994**, *35*, 1229.
(41) Minelli, M.; Giacinti Baschetti, M.; Hallinan, D. T.; Balsara, N. P. *J. Membr. Sci.* **2013**, *432*, 83−89.
(42) Sax, J.; Ottino, J. M. *Polym. Eng. Sci.* **1983**, *23*, 165.
(43) Shieh, J.-J.; Chung, T.-S.; Paul, D. R. *Chem. Eng. Sci.* **1999**, *54*, 675−684.
(44) Alam, T. M.; Hibbs, M. R. *Macromolecules* **2014**, *47*, 1073−1084.
(45) Fujimura, M.; Hashimoto, T.; Kawai, H. *Macromolecules* **1981**, *14*, 1309.
(46) Rae, P. J.; Dattelbaum, D. M. *Polymer* **2004**, *45*, 7615−7625.
(47) Hu, Y. S.; Liu, R. Y. F.; Rogunova, M.; Schiraldi, D. A.; Nazarenko, S.; Hiltner, A.; Baer, E. *J. Polym. Sci., Part B: Polym. Phys.* **2002**, *35*, 7326−7337.
(48) Modestino, M. A.; Kusoglu, A.; Hexemer, A.; Weber, A. Z.; Segalman, R. A. *Macromolecules* **2012**, *45*, 4681−4688.
(49) Page, K. A.; Cable, K. M.; Moore, R. B. *Macromolecules* **2005**, *38*, 6472−6484.

DOI: 10.1021/acs.macromol.5b00579
Macromolecules 2015, 48, 3303−3309